Int J Adv Manuf Technol (2018) 94:2861–2874
DOI 10.1007/s00170-017-1096-1

ORIGINAL ARTICLE

Spindle thermal error robust modeling using LASSO and LS-SVM

Feng Tan[1] · **Ming Yin**[1] · **Lin Wang**[1] · **Guofu Yin**[1]

Received: 19 April 2017 / Accepted: 12 September 2017 / Published online: 20 September 2017

Abstract To improve the spindle thermal error prediction accuracy, the least absolute shrinkage and selection operator (LASSO) is used to directly select the temperature-sensitive point subset to guarantee the prediction performance of the thermal error model built by least squares support vector machines (LS-SVM). Taking a horizontal machining center as a test stand, the thermal error experiments with different spindle speed states are carried out. Then the temperature-sensitive points are selected using LASSO. The number of temperature-sensitive points is reduced from 20 to 7. Afterward, the thermal error model is designed by LS-SVM. The prediction performance and generalization performance of the thermal error model are compared with another two thermal error models using gray model (GM) and multiple linear regression (MLR), respectively. The comparison results indicate that the thermal error model derived from LS-SVM shows better prediction performance and generalization performance than those derived from GM and MLR with the highest prediction accuracy increasing about 74.6 and 54.3%, respectively. Thus, the feasibility and effectiveness of the proposed spindle thermal error robust modeling method are validated.

Keywords Machine tool · Thermal error · Main spindle · LASSO · LS-SVM

✉ Ming Yin
mingyin@scu.edu.cn

[1] School of Manufacturing Science and Engineering, Sichuan University, Chengdu 610065, People's Republic of China

1 Introduction

With the development toward high speed and high precision of machine tools, many studies show that thermal error has become an increasing important factor affecting the machining accuracy of machine tools, which can account for up to 70% of total errors [1–3]. As the core component and the maximum heat source of machine tools, the spindle usually produces nonuniform temperature distribution and nonlinear thermal errors because of its complex structure, poor cooling conditions, and complex internal coupling relations [4], thus reducing the machining accuracy. Therefore, reducing the thermal error of machine tool spindle is crucial to improve the machining accuracy. Through symmetry designing, isolating heat sources, and using composite materials to construct the machine tools, the thermal deformations, and corresponding thermal errors can be radically reduced [5–7]. But this method is susceptible to hardware constraints and costly.

Accordingly, from the perspective of compensation, many scholars have studied to establish an accurate thermal error prediction model to compensate for the spindle thermal error. Some scientific publications predicted the thermal error through the established mechanism model of thermal deformation of machine tool spindles [8,9]. According to the thermo-elastic theory, as the spindle temperature increases, the spindle length increases [10]. The mechanism model was usually built based on that relationship. Creighton et al. [8] built a high-speed micro-milling spindle growth model through analyzing its thermal characteristics using FEM method and compensated the thermal error with that model. Wang et al. [9] simplified the *Z*-axis of a heavy boring and milling machine to a one-dimensional rod, and established the thermal error mechanism model through that one-dimensional rod. The results showed that the model is better than the output error model and the stepwise regression model. However,

through mechanism modeling, the original thermal deformation characteristics were simplified greatly, which could not accurately reflect the whole complex nonlinear thermal deformation process. Therefore, many scientific publications built machine tool thermal error prediction models from the mapping relationship between the temperature data in temperature-sensitive points and the thermal error data, and predicted the thermal error based on the real-time measured temperature values. Liang et al. [11] compared the robustness, versatility, and prediction accuracy of multivariate linear regression (MLR) model, back propagation (BP) neural network model, and radial basis function (RBF) neural network model in thermal error modeling and proved that both models had good effects. Guo et al. [12,13] screened temperature-sensitive points by gray correlation analysis and clustering analysis and established the prediction model using BP neural network with its parameters optimized by artificial fish swarm algorithm and ant colony algorithm. Ma et al. [14] used genetic algorithm and particle swarm optimization algorithm to optimize the initial weights, thresholds, and number of hidden layer neurons of a BP neural network thermal error model. Miao et al. [15] used traverse optimization method for selecting the optimum temperature measuring points and built a thermal error model using principal component regression algorithm. Wang et al. [16] used fuzzy *c* means (FCM) clustering method and the ISODATA method to select the temperature-sensitive points and verified the effectiveness of both methods. Cheng et al. [17] selected the temperature-sensitive points based on the rough set theory and constructed the thermal error model through RBF neural network method and BP neural network method, respectively.

The above modeling methods have achieved some good results, but there are still some shortcomings. The temperature-sensitive points are usually selected by clustering analysis and correlation analysis but independent to the modeling method itself; moreover, the temperature-sensitive points will change with the clustering number. The thermal error models using BP neural network are mainly built by optimizing their parameters through some optimization methods, but it is time consuming and may not guarantee the model with good generalization performance.

In the light of the temperature-sensitive point selection problem and the thermal error modeling problem of spindle thermal error, in this paper, the least absolute shrinkage and selection operator (LASSO) [18–20] is used to directly select the temperature-sensitive point subset and the least squares support vector machine (LS-SVM) [21] is used to derive the thermal error model, guaranteeing the robust prediction performance.

The framework of this paper is organized as follows: The thermal error experiments on different spindle speed states are conducted on a horizontal machining center in Section 2. In Section 3, the temperature-sensitive point subsets are selected by LASSO and evaluated with supervision. And the temperature-sensitive point subset ensuring the model with best prediction performance are selected as the temperature-sensitive points. Then in Section 4, the thermal error model is derived from LS-SVM and for comparison the thermal error models are also derived from gray model (GM) method [22,23] and MLR method. Afterward, in Section 5, the prediction performance and generalization performance of LS-SVM thermal error model are compared with those of the GM thermal error model and MLR thermal error model. The comparison results indicate that the LS-SVM thermal error model has the best prediction performance and generalization performance among the three thermal error models. Finally, the conclusions are made in Section 6.

2 Thermal error experiments

2.1 Experiment setup

In order to verify the feasibility and effectiveness of the proposed temperature-sensitive point selection method and thermal error modeling method, the spindle thermal error experiments of a horizontal machining center are carried out referring to ISO 230-3: 2007 [24] to obtain the temperature data and thermal error data. The experiment scheme is as follows:

The experiment setup is shown in Figs. 1 and 2. As shown in Fig. 1, altogether 20 temperature sensors are arranged on the machine tool. As specified in Table 1, T1–T7 are fixed on the outer surface of the front part of the spindle along its axis and T8–T10 are fixed on the outer surface of the rear part of the spindle along its axis to measure the spindle temperature in detail because it is the major heat source of the whole machine tool. T11–T13 are fixed on the side of the spindle box, T14–T16 are fixed on the side of the column, T17–T18 are fixed on the bed and T19 is fixed on the worktable, respectively. The ambient temperature is recorded by T20. All the temperature data are recorded in real time with 1 min interval. As shown in Fig. 2, a mandrel is clamped in the tool holder and three mutually perpendicular capacitive displacement sensors were fixed on the worktable to measure the thermal error of the spindle in three directions. The relative displacements between the mandrel and the three capacitive displacement sensors are regarded as the thermal errors of the spindle in three directions, respectively. Thus, the thermal elongation in the axial direction (*Z*-direction) and thermal drift in the radial directions (*X*- and *Y*-direction) can be measured. The thermal error data are recorded in real time with 1 min interval synchronously with temperature data. The measured temperature data and thermal error data at the same time was regarded as a sample.

A total of three thermal error experiments are conducted with three different spindle speed states, S = 2000 rpm,

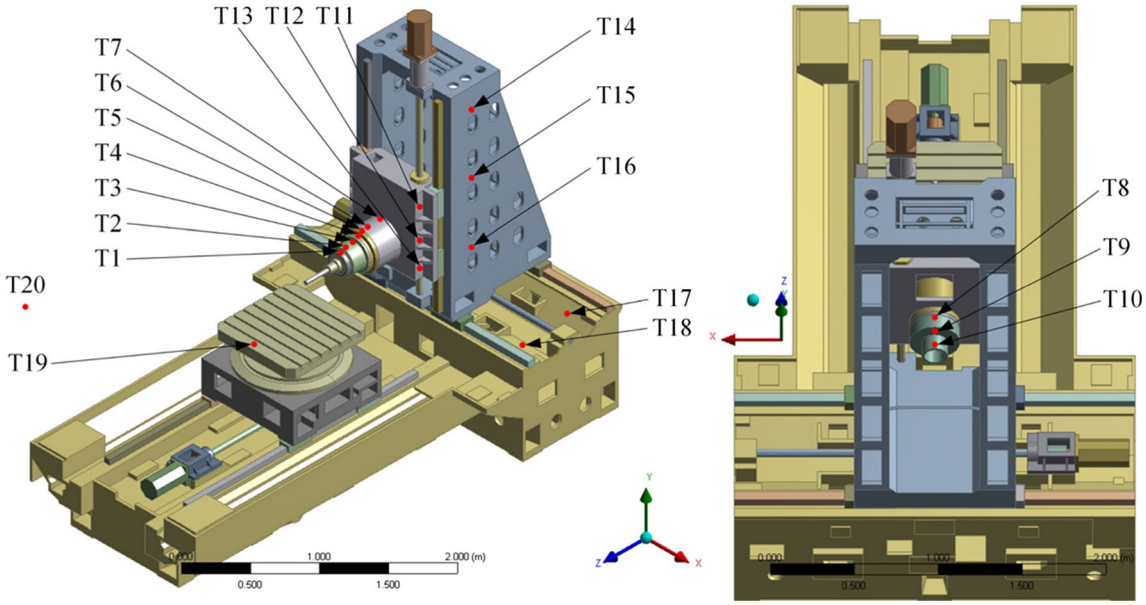

Fig. 1 Temperature sensors layout

$S = 4000$ rpm, and the speed spectrum shown in Fig. 3. During each experiment, the machine tool starts from the initial cold state and runs in NC-hold, without any movements at the set speed continuously for about 6 h without air conditioning and then stops. During the experiment, the temperature data and thermal error data are recorded in real time with an interval time of 1 min synchronously.

2.2 Experiment data

The collected temperature data and thermal error data are shown in Figs. 4 and 5, respectively, with a total $N = 360$ samples for each spindle speed state. As shown in Fig. 4, for all the three spindle speed states, the temperatures started rising from the initial cold state and finally reached a relative steady state. Different parts of the machine tool had different temperature rising trends. The closer the parts near the heat sources, the higher and faster the temperatures rise, and vice versa. As shown in Fig. 5, for all the three spindle speed states, the thermal error of the spindle mostly occurred in the axial direction (Z-direction), and the thermal error in the two radial directions (X- and Y-direction) are relatively small. Therefore, in this paper, only the thermal error in Z-direction of the spindle was considered for thermal error modeling, and in order to facilitate the description, the thermal error is denoted as y.

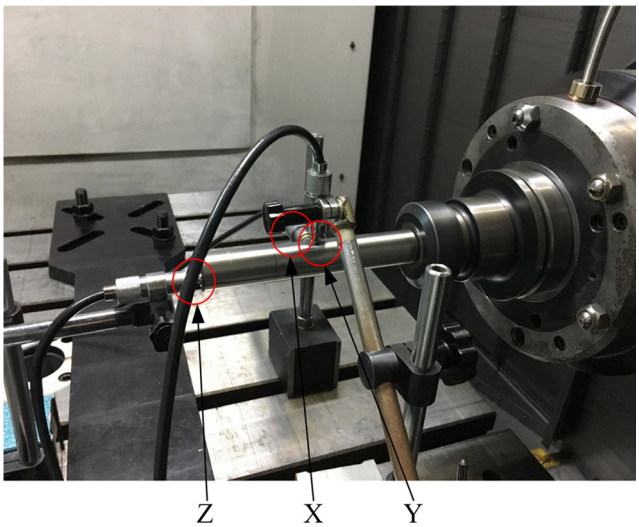

Fig. 2 Thermal error sensors layout

3 Temperature-sensitive point selection using LASSO

For simplifying the thermal error model and increasing its prediction ability meanwhile decreasing the measurement and compensation cost, the number of temperature points for modeling should be decreased. The temperature points used for modeling are usually named as thermal/temperature-sensitive points.

Table 1 Temperature sensors measurement locations

Temperature sensors	Measurement locations
T1–T7	Front part of the spindle
T8–T10	Rear part of the spindle
T11–T13	Side of the spindle box
T14–T16	Side of the column
T17, T18	Bed
T19	Worktable
T20	Ambient temperature

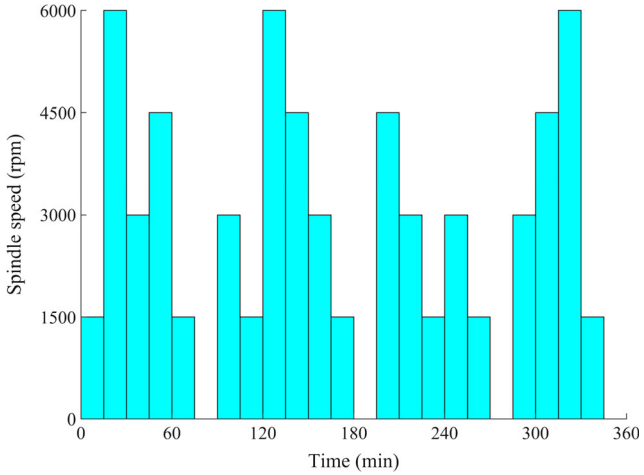

Fig. 3 Spindle speed spectrum

3.1 Temperature-sensitive point selection method

The traditional temperature-sensitive point selection method in machine tool thermal error modeling usually involved the combination of fuzzy clustering analysis and correlation analysis [12,13,16]. For example, fuzzy c means clustering analysis was one of the commonly used fuzzy clustering analysis method and the gray correlation analysis was one of the commonly used correlation analysis method in temperature-sensitive point selection. The full temperature points were clustered by the fuzzy c means clustering algorithm to reduce the collinearity between temperature-sensitive points, and then, in each cluster, the temperature point with the biggest degree of membership or with the biggest correlation coefficient with the thermal error was selected as a temperature-sensitive point.

However, the number of temperature-sensitive points is hard to decide with the traditional temperature-sensitive point selection method, as the number of temperature-sensitive points or the clustering number was usually specified by experience. As the clustering number changes, the new selected temperature-sensitive point subsets may not guarantee enhancing the prediction ability of the thermal error model. Moreover, the fuzzy clustering analysis is an unsupervised classification mechanism without using the information of the thermal error; thereby, the selected temperature-sensitive points may not be sensitive to the thermal error, and, further, cannot ensure enhancing the prediction ability of the thermal error model.

To solve the problem of selecting the best temperature-sensitive point combination thus enhancing the prediction ability of the thermal error model, the least absolute shrinkage and selection operator (LASSO) is adopted, here the presented research work. LASSO is a regression analysis method that performs variable selection to enhance the prediction accuracy and interpretability of the statistical model. It was introduced by Robert Tibshirani [18] in 1996. The basic idea of LASSO is to minimize the sum of squares of residuals under the constraint that the sum of the absolute values of the regression coefficients is less than a constant, thus producing some regression coefficients that are strictly equal to zero to achieve variable selection and obtain an interpretable model.

For a given nonnegative parameter λ, LASSO solves the following problem:

$$\min_{\beta_0,\boldsymbol{\beta}} \left(\frac{1}{2N} \sum_{i=1}^{N} \left(y_i - \beta_0 - \boldsymbol{x}_i^T \boldsymbol{\beta} \right)^2 + \lambda \sum_{j=1}^{p} \left| \beta_j \right| \right) \tag{1}$$

where the first part is the residual sum of squares for the regression, the second part is the penalty involving the L^1-norm of $\boldsymbol{\beta}$, N is the sample number of temperature data and thermal error data, y_i is the ith thermal error, $\boldsymbol{x}_i$ is the ith temperature data, a vector of p values, p is the total number of temperature points $p = 20$, the regression coefficients β_0 is a scalar and $\boldsymbol{\beta}$ is a vector of length p, respectively, and λ is the nonnegative regularization parameter which controls the amount of shrinkage that is applied to $\boldsymbol{\beta}$. As λ increases, the components of $\boldsymbol{\beta}$ shrink toward 0, and some components may be exactly equal to 0; thus, the number of nonzero components of $\boldsymbol{\beta}$ decreases. LASSO can effectively select a subset of the temperature points with enhanced prediction accuracy of the thermal error model.

The nonnegative regularization parameter sequence λ can be calculated as follows:

$$\lambda_i = e^{(\ln\lambda_{\max} + (i-1)\Delta_\lambda)} \left(i = 1, \ldots, n_\lambda \right) \tag{2}$$

$$\Delta_\lambda = -\frac{\ln\lambda_{\max} - \ln\lambda_{\min}}{n_\lambda - 1} \tag{3}$$

where n_λ is the number of the nonnegative regularization parameters, initially $n_\lambda = 100$, Δ_λ is the incremental interval of λ, and $\lambda_{\max}$ and $\lambda_{\min}$ are the maximum value and minimum value of λ, respectively, as follows:

$$\begin{cases} \lambda_{\max} = \dfrac{\max\left(\left| \boldsymbol{X}_0^T \boldsymbol{y}_0 \right| \right)}{N} \\ \lambda_{\min} = 0.0001\ \lambda_{\max} \end{cases} \tag{4}$$

where $\boldsymbol{X}_0$ is the standard score matrix of temperature data matrix $\boldsymbol{X}$ with the size of $N \times p$, $\boldsymbol{y}_0$ is the centralized vector of thermal error vector $\boldsymbol{y}$, $\boldsymbol{y}_0 = \boldsymbol{y} - \bar{y}$. After obtaining the nonnegative regularization parameter sequence λ, we can perform model fit and compute mean square error (MSE) for each λ. To improve the robustness and reduce the overfitting problem when computing the MSE, during the operation of LASSO, the MSE for each λ is computed with 10-fold cross-validation method [25]. Then the regression coefficients $\boldsymbol{\beta}$ corresponding

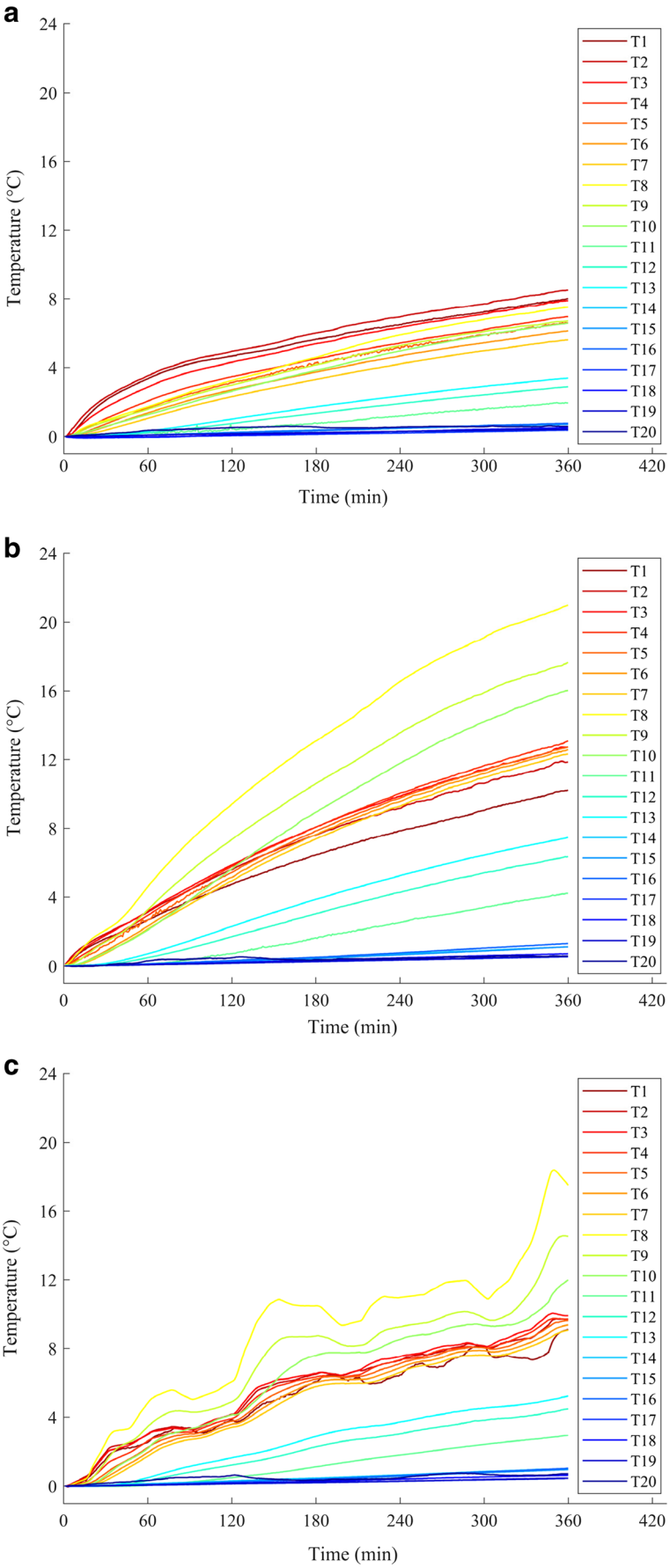

Fig. 4 **a** Temperature data with $S = 2000$ rpm. **b** Temperature data with $S = 4000$ rpm. **c** Temperature data with speed spectrum of Fig. 3

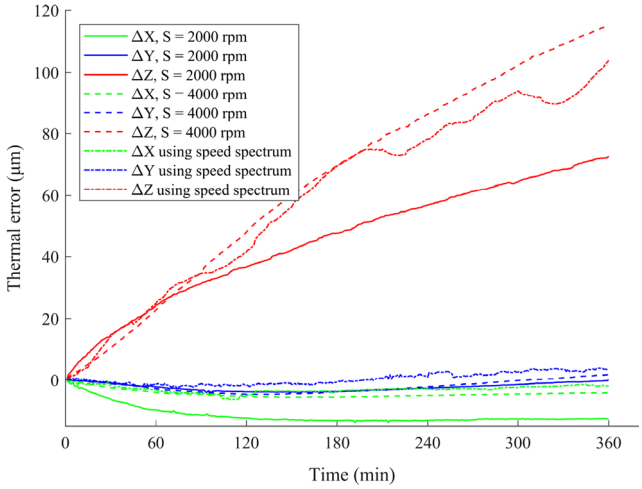

Fig. 5 Thermal error data

to the minimum solution for Eq. (1) for each λ can be solved by the iterative coordinate descent method [19,20]. Finally, select the regression coefficients $\boldsymbol{\beta}$ with minimum MSE, and the temperature points corresponding to the nonzero components in $\boldsymbol{\beta}$ can be picked out as the temperature-sensitive points.

3.2 Evaluation and selection of temperature-sensitive point subsets

We perform LASSO on the three groups of temperature data and thermal error data, respectively. The LASSO traces for the three group data are illustrated in Fig. 6. The value of the LASSO parameter λ increases from right to left along the bottom axis of abscissae. The degrees of freedom for the model, i.e., the number of nonzero regression coefficients, increases from left to right, along the top axis of abscissae. The left vertical axis shows the standardized coefficient values. With the increase of LASSO parameter λ, the components of coefficients shrank toward 0 and the nonzero coefficients appeared alternately. The dashed vertical line shows the λ value with minimum MSE and the corresponding nonzero coefficients are selected as the temperature-sensitive point subset. From Fig. 6, for each of the three group data, corresponding to minimum MSE, we pick out the temperature points with nonzero coefficients as the temperature-sensitive points and the selection results are summarized in Table 2. As shown, for the temperature data and thermal error data in S = 2000 rpm, T2, T4, T8, T14, T16, and T19 are chosen as temperature-sensitive points, for the temperature data and thermal error data in S = 4000 rpm, T1, T2, T6, T7, and T19 are chosen as temperature-sensitive points and for the speed spectrum shown in Fig. 3, T1, T3, T7, T8, T13, T16, and T20 are chosen as temperature-sensitive points. It indicates that with the change of the spindle speed state, the temperature-sensitive points vary. However, we can just pick out the best temperature-sensitive point subset insuring the best prediction accuracy by evaluating each subset.

For convenience, the MLR is taken as the regression model to evaluate the three temperature-sensitive point subsets. The expression of MLR is the following:

$$y = \beta_0 + \beta_1 x_1 + \ldots + \beta_m x_m \tag{5}$$

where y denotes the thermal error, x_i $(i = 1, \ldots, m)$ denotes the temperature value of the corresponding temperature-sensitive point selected by LASSO, m is the number of temperature-sensitive points in each subset, and $\boldsymbol{\beta} = (\beta_0, \beta_1, \ldots, \beta_m)$ are the regression coefficients and can be estimated by the least squares method, as follows:

$$\hat{\boldsymbol{\beta}} = \left(\boldsymbol{X}^T\boldsymbol{X}\right)^{-1}\boldsymbol{X}^T\boldsymbol{y} \tag{6}$$

where $\hat{\boldsymbol{\beta}}$ is the estimated regression coefficients vector with the length of $m + 1$, $\boldsymbol{X} = \{\mathbf{1}, \boldsymbol{x}_1, \boldsymbol{x}_2, \ldots, \boldsymbol{x}_m\}$ are the matrix with the size of $N \times (m + 1)$ consisting of a $\mathbf{1}$ vector with all the elements are 1 and the temperature values of temperature-sensitive points, and $\boldsymbol{y}$ is the thermal error vector with the length of N and N is the number of samples used for building the thermal error model.

For robustness, the evaluation of the three temperature-sensitive point subsets using MLR is 10-fold cross-validated using both three groups of temperature data and thermal error data. The collected total 360 data samples in each spindle speed state are randomly disturbed, and only the first 300 disturbed samples are used to evaluate the three temperature-sensitive point subsets. The evaluation results of the three temperature-sensitive point subsets are shown in Fig. 7. The vertical axis indicates the cross-validated root mean square error (RMSE). The smaller the RMSE is, the better the temperature-sensitive point subset is. As shown, for the data with the speed of S = 2000 rpm, both three temperature-sensitive point subsets almost have the same evaluation error with a slightly lower evaluation error in temperature-sensitive point subset 2. And for the data with the speed of S = 4000 rpm, the evaluation error of temperature-sensitive point subset 3 was slightly lower than that of subset 2 and both are much lower than that of subset 1. Finally, for the data with the speed spectrum shown in Fig. 3, the evaluation error of temperature-sensitive point subset 3 is lower than that of subset 2 and is further lower than that of subset 1. In general, temperature-sensitive point subset 3 shows the best results; thus, the corresponding temperature points in subset 3, T1, T3, T7, T8, T13, T16, and T20 are selected as the temperature-sensitive points for thermal error modeling with high prediction accuracy.

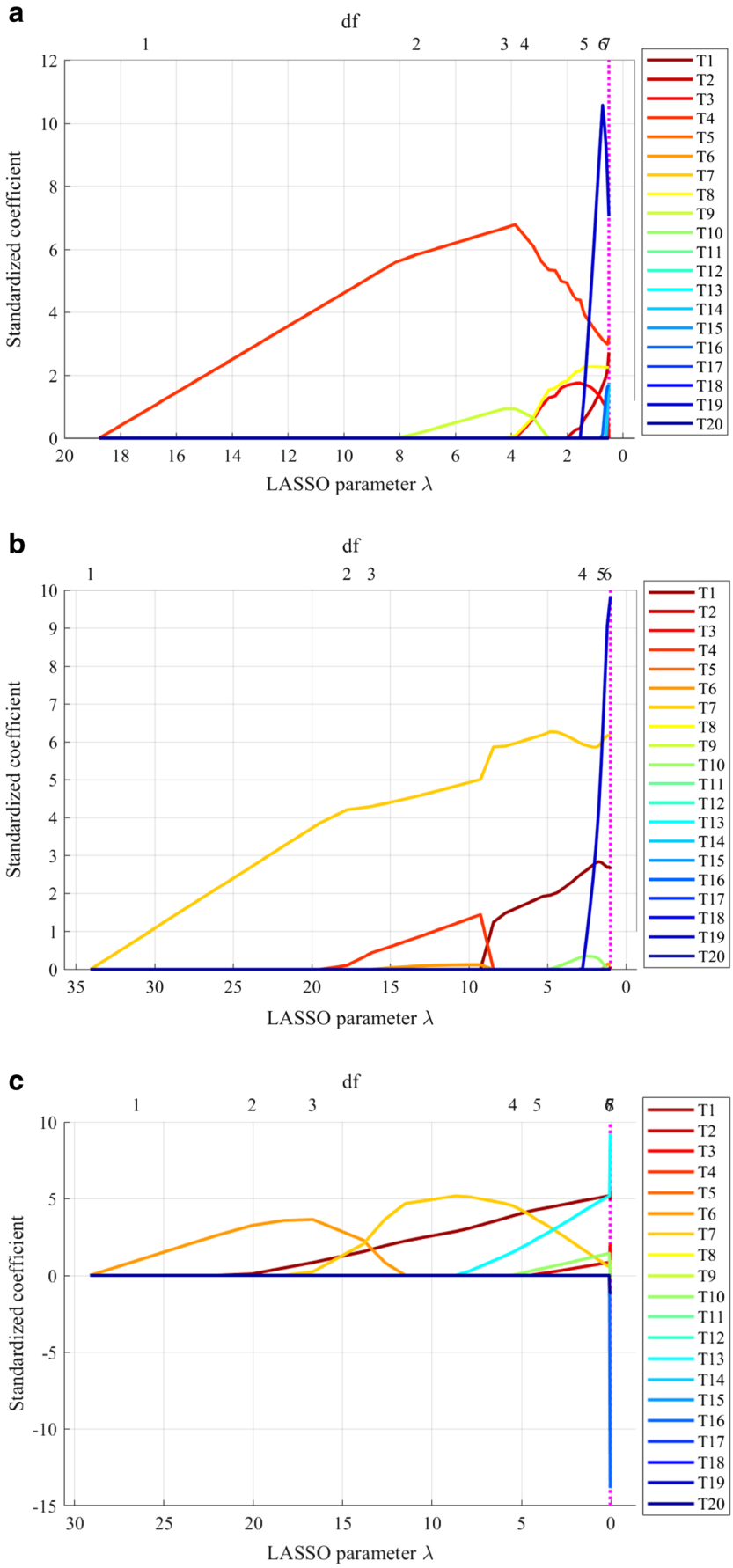

Fig. 6 **a** LASSO trace for the data with $S = 2000$ rpm. **b** LASSO trace for the data with $S = 4000$ rpm. **c** LASSO trace for the data with speed spectrum of Fig. 3

4 Thermal error modeling

4.1 Least squares support vector machine

The LS-SVM was proposed by J.A.K. Suykens et al. [21], which is a reformulation of the traditional SVM algorithm. The LS-SVM uses a regularized least squares function with equality constraints, leading to a linear system which meets the Karush-Kuhn-Tucker (KKT) conditions for obtaining an optimal solution. Consequently, the regression problem can be solved by a linear equation system rather than quadratic programming, as in SVM.

For the given temperature data matrix $\boldsymbol{X}$ of temperature-sensitive points and thermal error data vector $\boldsymbol{y}$ of the spindle Z-direction, the aim of LS-SVM is to construct the function $f(\boldsymbol{x}) = y$, which represents the dependence of the thermal error output y on the input temperature $\boldsymbol{x}$. The function of LS-SVM is formulated as follows:

$$f(\boldsymbol{x}) = \boldsymbol{w}^T \varphi(\boldsymbol{x}) + b \tag{7}$$

where $\boldsymbol{w}$ is the regression coefficients vector, $\varphi(\boldsymbol{x})$ is the nonlinear map function from original space to the high dimensional space and b is the constant model parameter. The optimization problem and the equality constraints of LS-SVM are defined as follows:

$$\left\{ \min_{\boldsymbol{w},\boldsymbol{e}} J(\boldsymbol{w},\boldsymbol{e}) = \frac{1}{2}\boldsymbol{w}^T\boldsymbol{w} + \frac{\gamma}{2}\sum_{i=1}^{n} e_i^2 \text{ s.t. } y_i = \boldsymbol{w}^T\varphi(\boldsymbol{x}_i) + b + e_i \right. \tag{8}$$

where $e_i (i = 1, \ldots, n)$ is the training error, n is the number of training samples, and γ is the tradeoff parameter between the solution size and training errors. The solution of Eq. (8) can be obtained by transforming it into the Lagrangian function, as follows:

$$L(\boldsymbol{w},\boldsymbol{e},b,\boldsymbol{\alpha}) = \frac{1}{2}\boldsymbol{w}^T\boldsymbol{w} + \frac{\gamma}{2} \times \sum_{i=1}^{n} e_i^2 - \sum_{i=1}^{n} \alpha_i \left[\boldsymbol{w}^T\varphi(\boldsymbol{x}_i) + b + e_i - y_i\right] \tag{9}$$

where $\alpha_i (i = 1, \ldots, n)$ is the is the Lagrangian multiplier. Then differentiate Eq. (9) with respect to $\boldsymbol{w}, \boldsymbol{e}, b, \boldsymbol{\alpha}$, respectively, and let the derivatives be zero, we obtain the following equations:

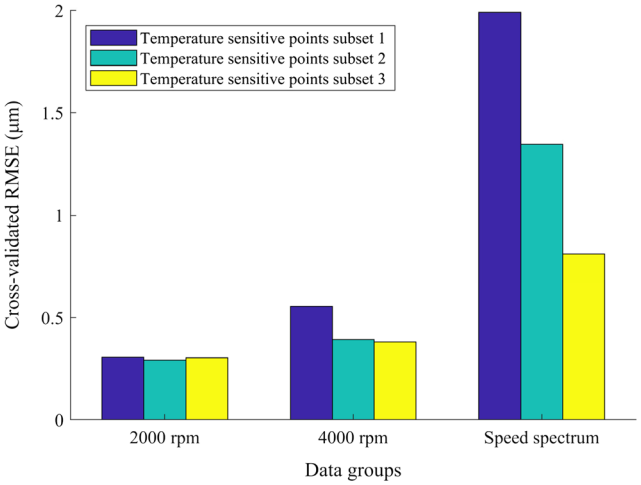

Fig. 7 Evaluation results of the temperature-sensitive points subsets

$$\begin{cases} \boldsymbol{w} = \sum_{i=1}^{n} \alpha_i \varphi(\boldsymbol{x}_i) \\ \sum_{i=1}^{n} \alpha_i = 0 \\ \alpha_i = \gamma e_i, \; i = 1, \ldots, n \\ y_i = \boldsymbol{w}^T\varphi(\boldsymbol{x}_i) + b + e_i, i = 1, \ldots, n \end{cases} \tag{10}$$

Eliminate $\boldsymbol{w}$ and $e_i (i = 1, \ldots, n)$ and define the kernel function $K(\boldsymbol{x}_i, \boldsymbol{x}_j) = \varphi(\boldsymbol{x}_i)^T\varphi(\boldsymbol{x}_j)$, the conditions for optimality lead to the following overall linear system instead of a quadratic programming problem, as follows:

$$\begin{bmatrix} 0 & 1 & \cdots & 1 \\ 1 & K(\boldsymbol{x}_1,\boldsymbol{x}_1) + 1/\gamma & \cdots & K(\boldsymbol{x}_1,\boldsymbol{x}_n) \\ \vdots & \vdots & \ddots & \vdots \\ 1 & K(\boldsymbol{x}_n,\boldsymbol{x}_1) & \cdots & K(\boldsymbol{x}_n,\boldsymbol{x}_n) + 1/\gamma \end{bmatrix} \begin{bmatrix} b \\ \alpha_1 \\ \vdots \\ \alpha_n \end{bmatrix} = \begin{bmatrix} 0 \\ y_1 \\ \vdots \\ y_n \end{bmatrix} \tag{11}$$

Usually, the Gaussian kernel function is used as the kernel function, as follows:

Table 2 Temperature-sensitive point subsets

Temperature-sensitive point subset	Temperature-sensitive points	λ
Subset 1 (2000 rpm)	T2, T4, T8, T14, T16, T19	0.4984
Subset 2 (4000 rpm)	T1, T2, T6, T7, T19	0.9934
Subset 3 (speed spectrum)	T1, T3, T7, T8, T13, T16, T20	0.0272

$$K(\boldsymbol{x}_i, \boldsymbol{x}_j) = \mathrm{e}^{\frac{-\|x_i - x_j\|^2}{2\sigma^2}} \tag{12}$$

where σ^2 is the kernel function parameter. The kernel function parameter σ^2 and the tradeoff parameter γ are the hyperparameters of LS-SVM. Given these two hyperparameters, the Lagrangian multipliers α_i $(i = 1, \ldots, n)$ and the constant model parameter b can be obtained from the solution of the linear equation system in Eq. (11). Thus, the final LS-SVM thermal error model can be derived from the rewritten form of Eq. (7) as a function of the Lagrangian multipliers, as follows:

$$f(\boldsymbol{x}) = \sum_{i=1}^{n} \alpha_i K(\boldsymbol{x}, \boldsymbol{x}_i) + b \tag{13}$$

4.2 Parameters determination

The performance of the LS-SVM depends on the two hyperparameters σ^2 and γ, and are usually obtained by grid search method which is very useful for small number of hyperparameters. Set the search range of the kernel function parameter σ^2 as (1, 2, …, 20) with spacing one and the search range of the tradeoff parameter γ as (50, 100, …, 1000) with spacing 50. Then, the LS-SVM thermal error model could be derived using the training temperature data and thermal error data with each combination of σ^2 and γ in the grid search ranges. For improving the prediction performance of the thermal error model, the temperature data and thermal error data in speed spectrum are used to build the thermal error model. The collected total N = 360 data samples in speed spectrum are randomly disturbed, and only the first 300 disturbed samples are used as the training data set as elaborated in Section 5. And then, take the mean prediction RMSE predicted using the data with S = 2000 rpm and S = 4000 rpm as the criterion to select the best hyperparameters. The grid search results of the two hyperparameters are shown in Fig. 8. As we can see, corresponding to the lowest RMSE denoted as the black point, $\sigma^2 = 2$ and $\gamma = 650$ are selected as the final hyperparameters. Once the two hyperparameters are obtained, the thermal error model could finally be built.

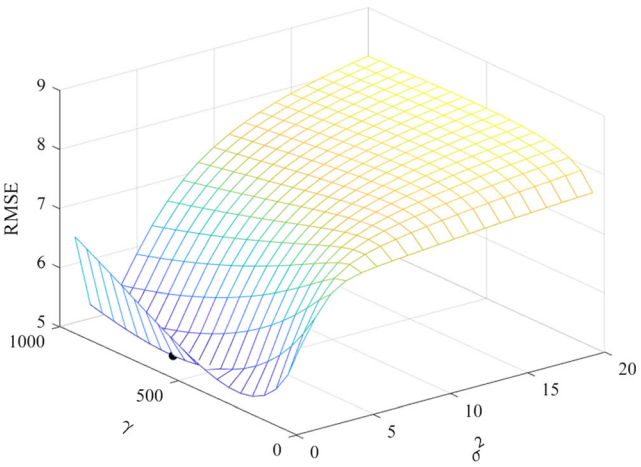

Fig. 8 Grid search results of hyperparameters σ^2 and γ

Table 3 Prediction accuracy comparison of different models using data with speed spectrum of Fig. 3

Model	Fitting RMSE (μm)	Fitting R^2	Test RMSE (μm)	Test R^2
LS-SVM	0.5738	0.9996	0.5838	0.9995
GM	1.1493	0.9985	0.9742	0.9985
MLR	0.9076	0.9991	0.8165	0.9989

5 Prediction performance analysis

5.1 Prediction performance

To obtain a LS-SVM thermal error model with strong generalization, the collected total N = 360 data samples using the speed spectrum of Fig. 3 are randomly disturbed. The first 300 disturbed samples are used as the training data set, and the remaining 60 disturbed samples are used as the test data set. Use the training data set and the hyperparameters to build the LS-SVM thermal error model and use the test data set to test the model. The fitting RMSE and test RMSE are shown in Table 3. The fitting RMSE refers to the prediction RMSE on the training data set and the test RMSE refers to the prediction RMSE on the test data set. For comparison, the GM method and the MLR method are also used to build the thermal error models. Their fitting RMSE and test RMSE are also shown in Table 3. As shown, all the models can fit on the training data

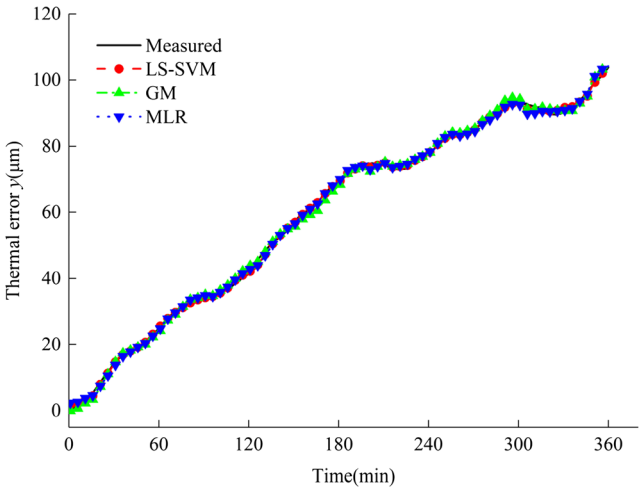

Fig. 9 Thermal error prediction curves with speed spectrum of Fig. 3

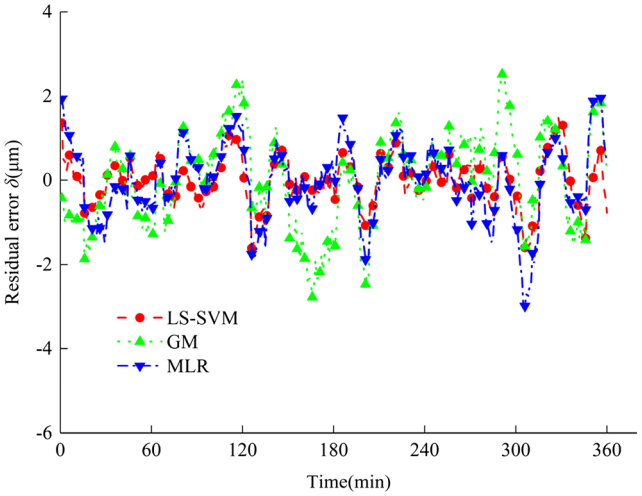

Fig. 10 Thermal error prediction residual error curves with speed spectrum of Fig. 3

and predict on the test data very well, and the best one is the LS-SVM model with the fitting RMSE about 0.5738 μm and test RMSE about 0.5838 μm, respectively.

The coefficient of determination R^2 of the models is also shown in Table 3. It indicates the proportionate amount of variation in the thermal error y explained by the temperature-sensitive points $\boldsymbol{x}$ in the thermal error model and ranges in (0, 1). The calculation of R^2 is shown in Eq. (14). The larger the R^2 is, the more variability is explained by the thermal error model. It is shown that all the three models had a close to 1 R^2 value in both the training data set and test data set, but the values obtained by the LS-SVM are slightly higher.

$$R^2 = \frac{\sum_{i=1}^{N}\left(\hat{y}_i - \bar{y}\right)^2}{\sum_{i=1}^{N}\left(y_i - \bar{y}\right)^2} \tag{14}$$

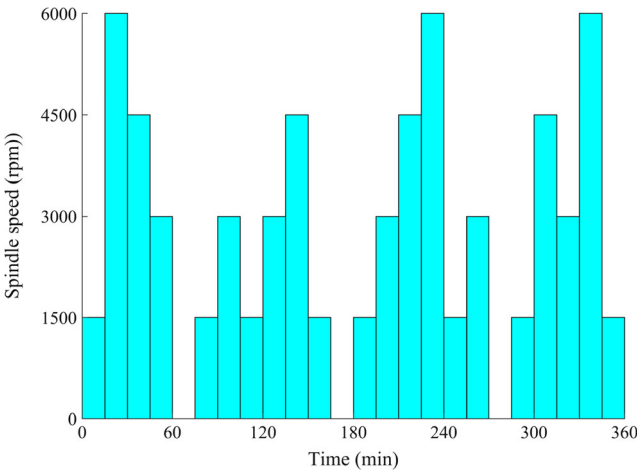

Fig. 11 New spindle speed spectrum

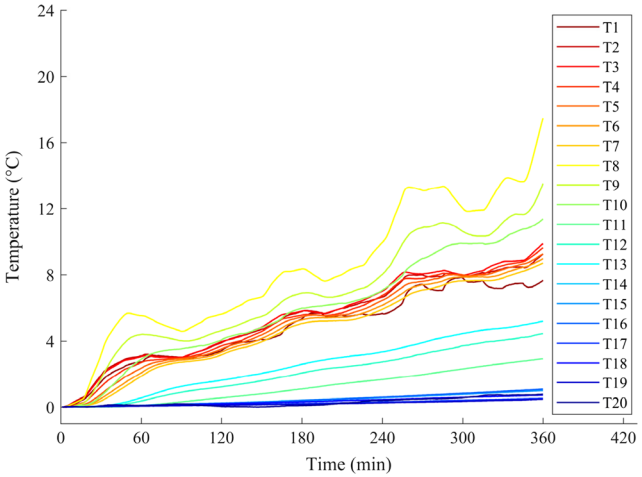

Fig. 12 Temperature data with new speed spectrumof Fig. 11

where y_i denotes the ith desired thermal error value, $\hat{y}_i$ denotes the ith predicted thermal error value, and $\bar{y}$ denotes the mean value of desired thermal error values.

The thermal error prediction curves for all training and test data of all three models are shown in Fig. 9. The three predicted thermal error curves by the three models are almost coincident with the measured thermal error curve. The thermal error prediction residual error curves of the three models are shown in Fig. 10. The residual error curves are almost distributed around the zero axis. All the three models have almost the same good prediction accuracy on the training data and test data from the same spindle speed spectrum. However, the prediction performance of a thermal error model mainly depends on its generalization performance, that is the ability to predict on new temperature data from different spindle speed.

5.2 Generalization performance

In order to verify the generalization performance of the LS-SVM thermal error model, the thermal errors are predicted on the temperature data with the spindle speed of S = 2000 rpm and S = 4000 rpm measured in Section 2 and the measured temperature data using a different spindle speed spectrum shown in Fig. 11. The new spindle speed spectrum is the reverse of the spindle speed spectrum in Fig. 3. Clearly, the spindle speed spectrum in Fig. 11 and the spindle speed spec-

Table 4 Prediction accuracy comparison of different models using data with S = 2000 rpm

Model	RMSE (μm)	R^2
LS-SVM	2.2731	0.9853
GM	8.9543	0.7725
MLR	4.9787	0.9297

Table 5 Prediction accuracy comparison of different models using data with S = 4000 rpm

Model	RMSE (μm)	R^2
LS-SVM	7.7523	0.9483
GM	11.1022	0.8939
MLR	13.3724	0.8461

trum in Fig. 3 are symmetric around the vertical axis. Under the same thermal error experiment setup as in Section 2, the thermal error experiment is conducted with the new spindle speed spectrum in Fig. 11. The measured temperature data with the new spindle speed spectrum are shown in Fig. 12.

Feeding the new data with S = 2000 rpm, S = 4000 rpm, and the new speed spectrum to the derived three thermal error models, respectively, and calculating the corresponding prediction errors, the prediction accuracies are listed in Tables 4, 5, and 6, respectively. As shown, for all the three different spindle speed states, the RMSEs of LS-SVM model are the lowest among the three prediction models with only about 2.2731 μm with S = 2000 rpm, 7.7523 μm with S = 4000 rpm, and 2.0318 μm with new speed spectrum. Comparing to GM and MLR, the prediction accuracy of LS-SVM increases by about 74.6 and 54.3% with S = 2000 rpm, 30.2 and 42.0% with S = 4000 rpm, and 55.4 and 38.4% with new speed spectrum, respectively. The coefficient of determination R^2 of the three models for all the three different spindle speed states are also shown in Tables 4, 5, and 6. As shown, for all the three different spindle speed states, the R^2 values of the LS-SVM model could maintain the highest among the three prediction models with about 0.9853 with S = 2000 rpm, 0.9483 with S = 4000 rpm, and 0.9947 with new speed spectrum. Therefore, the LS-SVM model can still hold good prediction performance when the spindle speed has changed, indicating that the LS-SVM model could maintain good generalization performance.

The thermal error prediction curves by the three models for all the three different spindle speed states are compared in Fig. 13. The thermal error curves predicted by LS-SVM model are in the best agreement with the measured thermal error curves for all the three different spindle speed states among the three models. The thermal error prediction residual error curves of the three models for all the three different spindle speed states are shown in Fig. 14. The residual error curves of the LS-SVM model for all the three different spindle speed states are the closest ones to the zero axis; on the contrary, the residual error curves of GM and MLR have seriously deviated from the zero axis. In general, all these indicate that the LS-SVM model has the best prediction performance and generalization performance among the three models, and is more suitable to be used as the thermal error prediction model in thermal error compensation.

Table 6 Prediction accuracy comparison of different models using data with new speed spectrum of Fig. 11

Model	RMSE (μm)	R^2
LS-SVM	2.0318	0.9947
GM	4.5606	0.9732
MLR	3.2967	0.9860

6 Conclusions

To further improve the spindle thermal error prediction accuracy, the LASSO was used to select the temperature-sensitive point subsets and the LS-SVM was used to derive the thermal error model. The spindle thermal error experiments were conducted on a horizontal machining center at three spindle speed states, S = 2000 rpm, S = 4000 rpm, and speed spectrum. The temperature-sensitive points varied with the change of the spindle speed state, and three different temperature-sensitive point subsets were selected by LASSO using the data in the three different spindle speed states. Through evaluation by MLR, the final seven temperature points T1, T3, T7, T8, T13, T16, and T20 were picked out as the temperature-sensitive points. Compared with the conventional unsupervised method using fuzzy clustering analysis and correlation analysis, the proposed temperature-sensitive point selection method using LASSO is a kind of supervised method and can select the best temperature-sensitive point subset with the number of temperature-sensitive points automatically determined. By regarding the temperature-sensitive points as the input variables and the thermal error as the output variable, the thermal error model was derived from LS-SVM using the temperature data and thermal error data with speed spectrum. Thereafter, the prediction performance and generalization performance of the thermal error model derived from LS-SVM were compared with those of the thermal error models derived from the commonly used GM and MLR, respectively. The comparison results indicated that thermal error model derived from LS-SVM had the best prediction performance and generalization performance with the highest prediction accuracy increasing about 74.6 and 54.3% compared with GM and MLR, respectively. The feasibility and superiority of the proposed temperature-sensitive point selection method and thermal error modeling method are verified. Using the proposed method, the spindle thermal error model with better prediction performance can be built; thus, the spindle thermal error can be compensated more effectively. The proposed method may provide an alternative in thermal error modeling for machine tool researchers, manufacturers, and users. All the work prepares for the subsequent implementation of thermal error compensation.

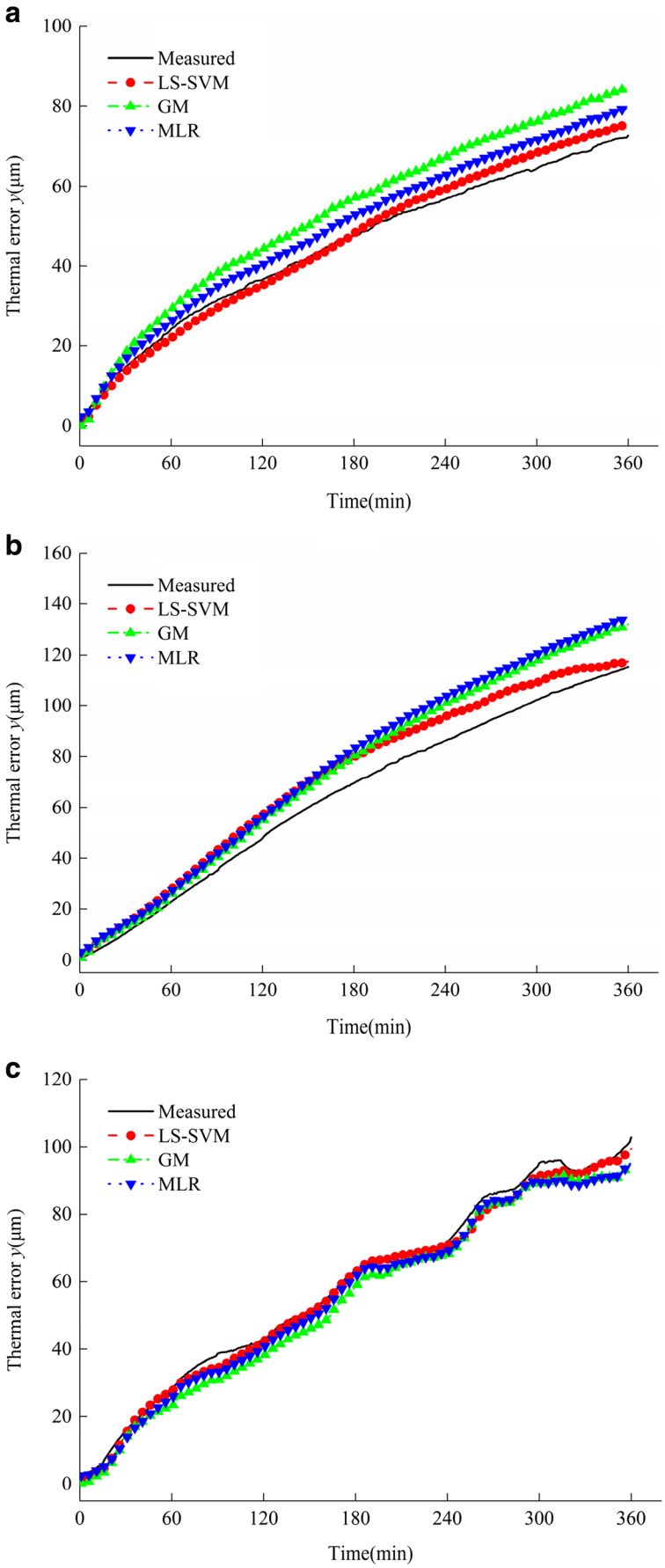

Fig. 13 **a** Thermal error prediction curves with $S = 2000$ rpm. **b** Thermal error prediction curves with $S = 4000$ rpm. **c** Thermal error prediction curves with new speed spectrum of Fig. 11

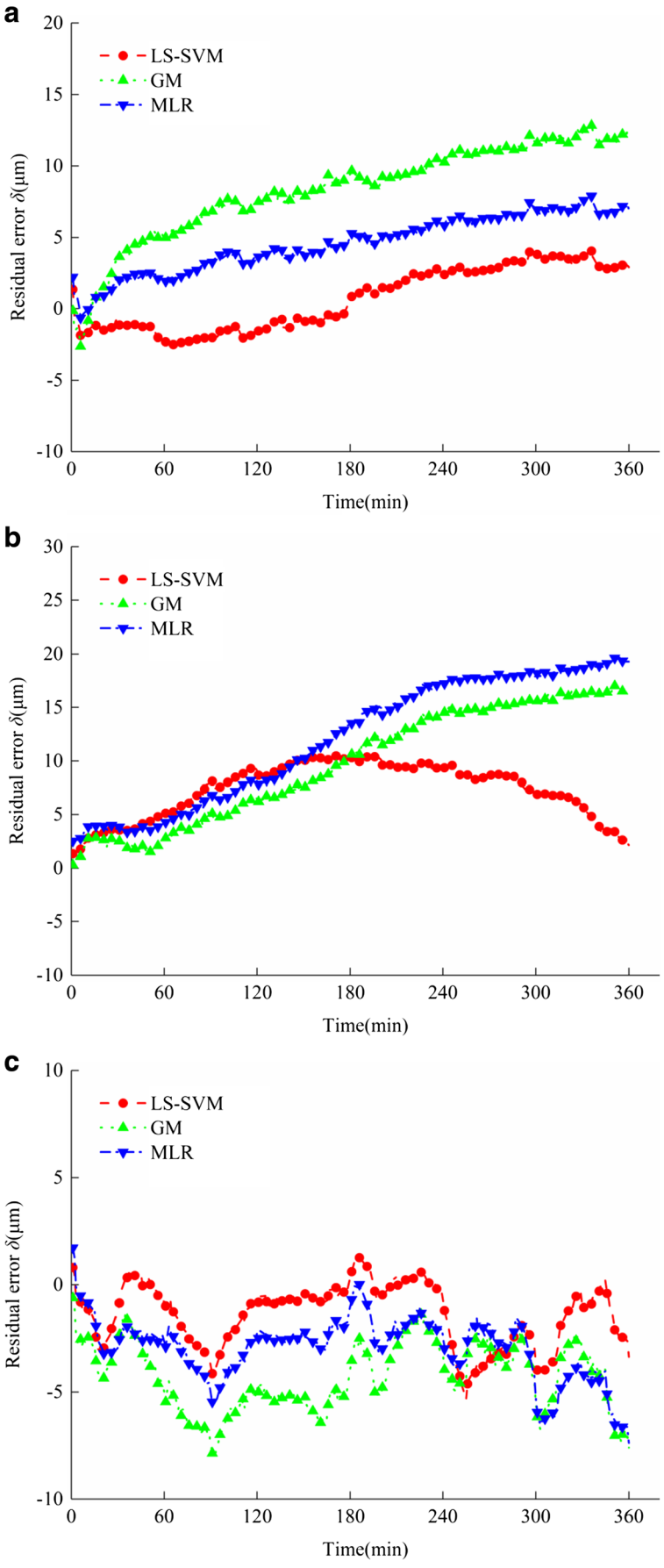

Fig. 14 **a** Thermal error prediction residual error curves with $S = 2000$ rpm. **b** Thermal error prediction residual error curves with $S = 4000$ rpm. **c** Thermal error prediction residual error curves with new speed spectrum of Fig. 11

Acknowledgments This research was financially supported by the Key National Science and Technology Projects of China (grant no. 2015BAF02B02) and the Science and Technology Support Plan Project of Sichuan province, China (grant no. 2015GZ0030).

References

1. Ramesh R, Mannan MA, Poo AN (2000) Error compensation in machine tools—a review: part II: thermal errors. Int J Mach Tools Manuf 40(9):1257–1284
2. Mayr J, Jedrzejewski J, Uhlmann E, Alkan Donmez M, Knapp W, Hartig F, Wendt K, Moriwaki T, Shore P, Schmitt R (2012) Thermal issues in machine tools. CIRP Ann Manuf Technol 61(2):771–791
3. Li Y, Zhao WH, Lan SH, Ni J, Wu WW, Lu BH (2015) A review on spindle thermal error compensation in machine tools. Int J Mach Tools Manuf 95:20–38
4. Cao HR, Zhang XW, Chen XF (2016) The concept and progress of intelligent spindles: a review. Int J Mach Tools Manuf 112:21–52
5. Abdulshahed AM, Longstall AP, Fletcher S (2015) The application of ANFIS prediction models for thermal error compensation on CNC machine tools. Appl Soft Comput 27:158–168
6. Tan F, Yin GF, Yin Q, Dong GH, Wang L (2016) CNC machine tool thermal error modeling based on GM-LS-SVM hierarchical model. J Central South Univ (Sci and Technol) 12:4028–4034 **(in Chinese)**
7. Sun LJ, Ren MJ, Hong HB, Yin YH (2017) Thermal error reduction based on thermodynamics structure optimization method for an ultra-precision machine tool. Int J Adv Manuf Technol 88(5–8): 1267–1277
8. Creighton E, Honegger A, Tulsian A, Mukhopadhyaye D (2010) Analysis of thermal errors in a high-speed micro-milling spindle. Int J Mach Tools Manuf 50(4):386–393
9. Wang LP, Wang HT, Li TM, Li FC (2015) A hybrid thermal error modeling method of heavy machine tools in z-axis. Int J Adv Manuf Technol 80(1–4):389–400
10. Holman JP (2010) Heat transfer. McGraw-Hill
11. Liang RJ, Ye WH, Zhang HY, Yang QF (2012) The thermal error optimization models for CNC machine tools. Int J Adv Manuf Technol 63(9–12):1167–1176
12. Guo QJ, Yang JG, Wu H (2010) Application of ACO-BPN to thermal error modeling of NC machine tool. Int J Adv Manuf Technol 50(5):667–675
13. Guo QJ, Xu RF, Yang TY, He L, Cheng X, Li ZY, Yang JG (2016) Application of GRAM and AFSACA-BPN to thermal error optimization modeling of CNC machine tools. Int J Adv Manuf Technol 83(5–8):995–1002
14. Ma C, Zhao L, Mei XS, Shi H, Yang J (2017) Thermal error compensation of high-speed spindle system based on a modified BP neural network. Int J Adv Manuf Technol 89(9–12):3071–3085
15. Miao EM, Liu Y, Liu H, Gao ZH, Li W (2015) Study on the effects of changes in temperature-sensitive points on thermal error compensation model for CNC machine tool. Int J Adv Manuf Technol 97:50–59
16. Wang HT, Wang LP, Li TM, Han J (2013) Thermal sensor selection for the thermal error modeling of machine tool based on the fuzzy clustering method. Int J Adv Manuf Technol 69(1):121–126
17. Cheng Q, Qi Z, Zhang GJ, Zhao YS, Sun BW, Gu PH (2016) Robust modelling and prediction of thermally induced positional error based on grey rough set theory and neural networks. Int J Adv Manuf Technol 83(5):1–12
18. Tibshirani R (1996) Regression shrinkage and selection via the lasso. J. R. Statist. Soc. B 58(1):267–288
19. Friedman J, Hastie T, Tibshirani R (2010) Regularization paths for generalized linear models via coordinate descent. J Statist Soft 33(1):1–22
20. Zou H, Hastie T (2005) Regularization and variable selection via the elastic net. J R Statist Soc B 67(2):301–320
21. Suykens J A K, Van Gestel T, De Brabanter J (2002) Least squares support vector machines. World Scientific
22. Liu SF, Dang YG, Fang ZG (2010) Gray system theory and its application. Science Press, Beijing
23. Zhang Y, Yang JG, Jiang H (2012) Machine tool thermal error modeling and prediction by grey neural network. Int J Adv Manuf Technol 59(9):1065–1072
24. ISO 230-3 (2007) Test code for machine tools part 3: determination of thermal effects. ISO copyright office, Geneva
25. Geisser S (1993) Predictive inference. CRC press